OPEN ACCESS

Comparison of Ionic Transport Properties of Non-Aqueous Lithium and Sodium Hexafluorophosphate Electrolytes

To cite this article: Johannes Landesfeind *et al* 2021 *J. Electrochem. Soc.* **168** 040538

Journal of The Electrochemical Society, 2021 **168** 040538

Comparison of Ionic Transport Properties of Non-Aqueous Lithium and Sodium Hexafluorophosphate Electrolytes

Johannes Landesfeind,[1,z] Tomooki Hosaka,[2] Maximilian Graf,[1,*] Kei Kubota,[2] Shinichi Komaba,[2,] and Hubert A. Gasteiger[1,***]**

[1]*Chair of Technical Electrochemistry, Department of Chemistry and Catalysis Research Center, Technical University of Munich, Munich, Germany*
[2]*Department of Applied Chemistry, Tokyo University of Science, Tokyo, Japan*

To bridge the gap between current lithium-ion battery technology and alternative cell chemistries such as, e.g., sodium-ion batteries, the majority of the research in this field focuses on the improvement of the cell's energy density by the development of new active materials for reversible storage of sodium ions. On the other hand, the power density, which is determined by the ionic transport and thermodynamic parameters in the electrolyte, namely the conductivity, the thermodynamic factor, the transference number, and the diffusion coefficient, is attracting little attention. In this contribution, we determine these electrolyte properties for 0.1 M to 2 M $LiPF_6$ and $NaPF_6$ in a mixture of ethylene carbonate and diethyl carbonate (EC:DEC (1:1 v:v)) and use them in 1D simulations to show their impact on the theoretical discharge rate performance of the lithium and sodium cell chemistry. We show that the increased cation size of sodium and its corresponding weaker solvent interactions are beneficial for high power applications and that the improved ionic transport properties would allow for a substantial increase of either the (dis)charge currents or the electrode areal loading, compared to the well-established lithium system.
 [DOI: 10.1149/1945-7111/abf8d9]

Manuscript submitted February 27, 2021; revised manuscript received April 3, 2021. Published April 29, 2021. *This was Paper 211 presented at the New Orleans, Louisiana, Meeting of the Society, May 28–June 1, 2017.*

Supplementary material for this article is available online

Sodium-ion and potassium-ion secondary batteries, as alternatives to the currently utilized lithium-ion technology, attract growing interest in the research community.[1–6] The higher abundance of these alkali metals compared to lithium, their consequently lower cost, the possibility to replace the expensive copper current collector of lithium-ion battery (LIB) anodes by cheaper aluminum,[1] and the reduced standard potential of potassium in non-aqueous solvents compared to lithium[7] make them a potential candidate for future electric storage applications in, e.g., electric cars or mobile phones. Established in 1988 with the first demonstration of a sodium ion full cell,[8] sodium-ion batteries have been improved steadily and have been demonstrated as alternatives for lithium-ion batteries.[9–11] One of the few comparative studies of the electrolyte parameters of lithium and sodium salts in aprotic solvents by Matsuda et al. report conductivity, viscosity, and coordination number for $LiClO_4$, $NaClO_4$, and $KClO_4$ in mixtures of propylene carbonate (PC) and 1,2-dimethoxyethane (DME).[12] Similar studies were done by Kuratani et al.[13] and Ponrouch et al.[14] The desolvation energies of Li^+, Na^+, and K^+ ions based on DFT calculations for a large number of aprotic solvents follow the order Li > Na > K and are attributed to the decrease of the cations' Lewis acidity;[15] similarly, the Stokes radius was found to decrease in the same order (Li > Na > K).[12] An extensive study of the solvation structure of lithium and sodium hexafluorophosphate salts in various solvents employing multiple experimental techniques, including Raman spectroscopy and NMR spectroscopy, examines the extent of ion-ion and ion-solvent interactions and reports higher mobilities of $NaPF_6$ compared to $LiPF_6$ in mixtures of EC and ethyl methyl carbonate (EMC).[16]

While the above studies investigate some chemical or individual transport properties of aprotic electrolytes, a more comprehensive understanding of the ion transport in the electrolyte can only be obtained by determining all ionic transport and thermodynamic properties. I.e., in addition to the commonly reported conductivity (κ), detailed knowledge about the thermodynamic factor (TDF $\equiv 1 + d\ln[f_\pm]/d\ln[c]$, i.e., a derivative form of the mean ionic activity coefficient ($f_\pm$) with concentration), the cation transference number (t_+), and the binary diffusion coefficient ($D_\pm$) arerequired as well. Because they are very "*cumbersome to attain*,"[17] the literature lacks comparative studies of these electrolyte parameters in aprotic solvents with different alkali ion salts, which is particularly unsatisfactory as the different cation-solvent interactions are likely to have a big influence on ion transport. For example, ion-ion interactions are reduced by 20% when exchanging lithium for sodium ions in an electrolyte, and coordination numbers and solvation structures differ due to the different charge/radius ratios of the cations and their different Lewis acidities.[18] Because the electrolyte parameters are directly or indirectly affected by the solvation shell around the cation (its mobility affects conductivity, transference number, and diffusion coefficient) and impacts the energy required to remove the cation from its solvation shell (related to the thermodynamic factor), comparative studies of electrolyte parameters for different alkali ions are of great interest.

Recently, we introduced and applied novel and existing methods to determine all relevant electrolyte parameters in non-aqueous electrolytes.[19–21] In addition to the straightforward measurement of the ionic conductivity, we described the determination of the binary diffusion coefficient from galvanostatic pulse experiments,[19] as well as the determination of transference numbers and thermodynamic factors based on concentration cell potentials and the short term potential relaxation after current pulses in symmetric lithium cells.[21] In this work, we apply the same methodology to 0.1−2 M $LiPF_6$ and 0.1−2 M $NaPF_6$ in EC:DEC (1:1 v:v). For a detailed description of the theory and data analysis, the interested reader is referred to our recent publication[21] and we limit ourselves here to a brief overview of the respective parameter determination methods, showing exemplary data in the supporting information. The choice of salt and solvent is based on commonly used electrolyte compositions in lithium-ion batteries and on the reported stable cycling of sodium-ion batteries for this electrolyte.[9]

In the *Experimental* section, all procedures, as well as the used materials and devices, are introduced only if they differ from the original methodology, otherwise, the reader is referred to our

*Electrochemical Society Student Member.
**Electrochemical Society Member.
***Electrochemical Society Fellow.
[z]E-mail: j.landesfeind@tum.de

previous work.[19,21] The obtained transport (κ, $D_{\pm}$, and, t_+) and thermodynamic (TDF) parameters in the section *Results and Discussion* are compared to literature values of aqueous LiCl, NaCl, and KCl electrolytes to compare the various parameter trends. Concentration dependent functional descriptions of these parameters are fitted to experimental data and are summarized in Table I. At last, we use the determined electrolyte parameters to model the discharge behavior of a hypothetical "NMC/graphite" full cell (i.e., using the characteristic open circuit potential vs capacity and the characteristic kinetics of a lithium-ion battery with NCM and graphite) and elaborate on the impact of the electrolyte parameters on the cell's power performance.

Experimental

A mixture of ethylene carbonate and diethyl carbonate (EC:DEC 1:1 v:v, Kishida Chemical, >99.5%) was used as a solvent for self-prepared electrolytes containing 0.1 M, 0.5 M, 1.0 M, 1.5 M, and 2.0 M lithium hexafluorophosphate ($LiPF_6$, BASF, battery grade) or sodium hexafluorophosphate ($NaPF_6$, Kishida Chemical, battery grade) salt. Electrolytes were mixed in an argon-filled glovebox (temperature 25 °C ± 1 °C, glovebox from MBraun, water content <0.1 ppm, Ar 5.0, Westfalen, 99.999% Vol). Throughout this study, we use M to denote volumetric salt concentrations, i.e., moles per liter. With the Karl-Fischer technique, we found water contents below 12 ppm for the 2 M electrolytes. Metallic lithium (Rockwood Lithium, 75 μm thickness, high purity, 99.9%) or sodium (Sigma Aldrich, cubes, in mineral oil, 99.9%) was used for the electrodes. All cell parts were cleaned by boiling them in a mixture of ethanol and water (Millipore, Elix, 15 MΩ), thoroughly rinsing them with water, followed by overnight drying at 70 °C in a heating oven before bringing them into the glove box.

The electrolyte conductivities were measured at 25 °C inside the glovebox using a commercially available conductivity sensor (SI Analytics, LF 1100 T+) in a glass cell. Concentration potentials were measured inside the glovebox using a concentration cell setup consisting of two glass plates, a glass fiber separator (VWR, thickness 250 μm, borosilicate, binder-free), and two metallic lithium or sodium electrodes, as described in detail in Ref. 20. To obtain clean sodium electrodes, all sides of the sodium metal cube were cut to avoid contaminations with mineral oil, and the clean sodium metal piece was rolled inside a polypropylene plastic bag to prepare a flat foil; the lithium was used as-received.

The setup for galvanostatic pulse experiments only differs slightly from the symmetric lithium coin cell setup described in Ref. 21. In the present work, circular lithium or sodium disks of 14 or 16 mm diameter ($A_{El.}$ = 1.54 or 2.01 cm^2) were punched for use as counter and working electrodes (CE and WE) in a symmetric cell configuration (i.e., either two lithium electrodes with the lithium electrolyte or two sodium electrodes with the sodium electrolyte). The lithium or sodium electrodes were separated by a circular disk (16 mm diameter) of a porous polypropylene sheet with $l_{Sep.}$ = 500 μm thickness (Sunmap LC, polypropylene, $\varepsilon_{Sep.}$= 30% porosity, 17 μm pore size, Nitto, Japan). Compared to the setup described in our recently published study,[21] the electrode and separator diameters are smaller, and the separator was not plasma treated (using larger electrodes, a separator with a slightly larger diameter than the electrodes, and a plasma-treated separator were modifications to improve the reliability of the measurement setup that we had only introduced after the measurements shown in the present study). The tortuosity of the porous sheet, in the following called separator, was determined to be 4.8 ± 0.4 (described at the end of the *Experimental* section in Ref. 21). The coin cells were assembled inside the glovebox using one or two 0.5 mm spacers, a 1.4 mm washer, and an electrolyte volume of 40 μl (corresponding to 4/3 of the separator void volume). As it was found to improve the stability of the sodium/sodium cells in the galvanostatic pulse experiments 5% FEC (by mass) was added to the sodium electrolytes for the coin cell experiments (no FEC was necessary for conductivity and concentration cell measurements). As this additive concentration is small it is not expected to alter the transport properties of the sodium electrolytes significantly but mostly supports the formation of a more stable passivation at the sodium/electrolyte interface. After the coin cells were sealed, measurements were done at 25 °C in a climate chamber outside the glovebox. The measurement procedure consisted of a 30 min resting phase, a 15 min galvanostatic pulse, and a 3–5 h OCV (open circuit voltage) phase to observe the relaxation of the cell potential. In total four current pulses with alternating signs were applied to at least two cells for each electrolyte. Table S1 in the Supporting Information (available online at stacks.iop.org/JES/168/040538/mmedia) summarizes the current densities used in the galvanostatic pulse experiments. Compared to the lithium/lithium cells much smaller currents were used for the sodium/sodium cells to avoid the formation of dendritic structures. A Biologic VMP3 potentiostat/galvanostat was used for the electrochemical measurement of concentration cells and pulse experiments.

Results and Discussion

In the following section, we present the measurement results for the ionic conductivity, the binary diffusion coefficient (following the methodology introduced in Ref. 19), the thermodynamic factor, and the transference number (following the methodology introduced in Ref. 21) for 0.1-2.0 M $LiPF_6$ and $NaPF_6$ in EC:DEC (1:1 v:v) at 25 °C. As the measurement techniques have been introduced in great detail in the given references, this publication focuses on the

Table I. Empirical fitting equations and fitted dimensionless parameters, including their confidence interval based on a 90% confidence interval, describing the concentration dependence of the transport and thermodynamic parameters for $LiPF_6$ and $NaPF_6$ in EC:DEC (1:1 v:v, 5 wt% FEC was added to sodium electrolytes in coin cells). These are shown by the solid lines in Figs. 1a, 2a, Figs. 3a, and 4a. Concentrations are used in units of moles per liter.

Empirical function		$LiPF_6$	$NaPF_6$
$\kappa(c) = p_1 \cdot c \cdot \frac{1 + p_2 \cdot \sqrt{c} + p_3 \cdot c}{1 + \exp(p_4 \cdot c^2)} \cdot \frac{\text{mS}}{\text{cm}}$	p_1	6.30E+01(± 3.3E+01)	6.12E+01(± 1.6E+01)
	p_2	−7.77E-01(± 4.2E-01)	−7.32E-01(± 1.7E-01)
	p_3	2.02E-01(± 3.1E-01)	8.57E-02(± 1.8E-01)
	p_4	7.63E-01(± 4.0E-01)	3.74E-01(± 5.8E-01)
$\text{TDF} \equiv \left(1 + \frac{\text{d} \ln f_{\pm}(c)}{\text{d} \ln c}\right) = p_1 + p_2 \cdot c$	p_1	6.16E-01(± 2.6E-01)	1.24E+00(± 6.9E-02)
	p_2	1.17E+00(± 2.2E-01)	3.06E-01(± 5.8E-02)
$t_+(c) = p_1 + p_2 \cdot c$	p_1	1.90E-01(± 1.0E-01)	5.26E-01(± 2.8E-02)
	p_2	−7.72E-02(± 8.5E-02)	−1.32E-01(± 2.3E-02)
$D_{\pm}(c) = p_1 \cdot \exp(p_2 \cdot c) \cdot 10^{-6} \frac{\text{cm}^2}{\text{s}}$	p_1	4.44E-06(± 1.6E-07)	4.07E-06(± 2.2E-07)
	p_2	−6.17E-01(± 4.7E-02)	−3.67E-01(± 4.1E-02)

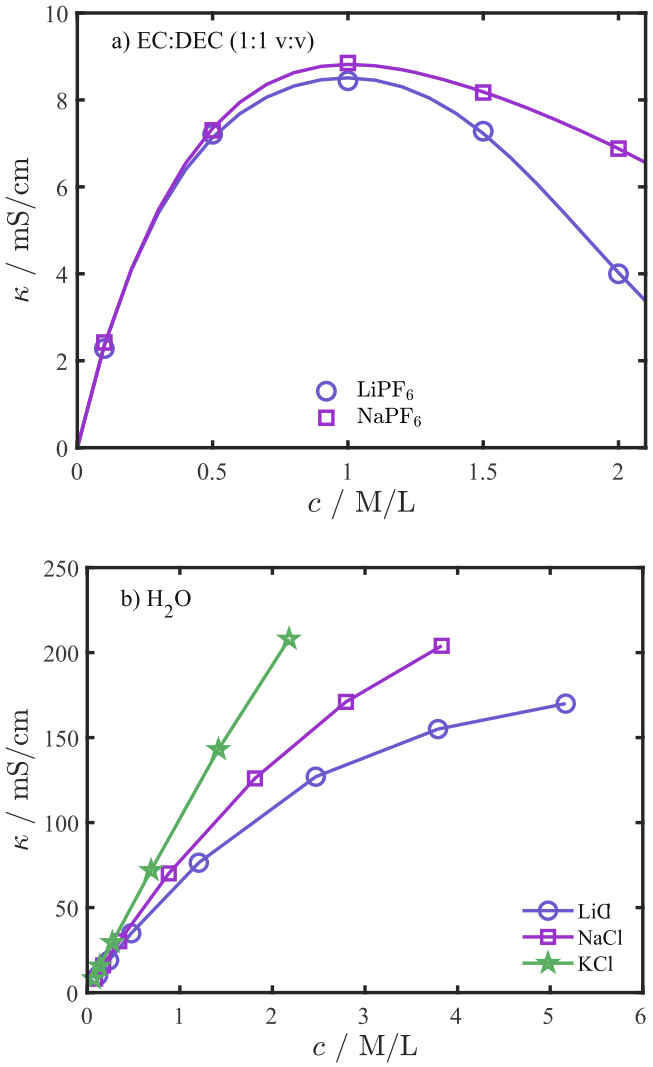

Figure 1. Ionic conductivity of (a) $LiPF_6$ (blue circles) and $NaPF_6$ (purple squares) solutions in EC:DEC (1:1 v:v) measured at 25 °C; solid lines represent fits to the conductivity equation given in Table I (fitting parameters and their confidence intervals are also given in the table); (b) Aqueous LiCl (blue circles), NaCl (purple squares), and KCl (green stars) electrolytes at 25 °C (data are taken from Ref. 22 and transformed into molarities with assumed linear densities from Ref. 23); solid lines in (b) serve as a guide to the eye.

observed differences of the ionic transport and the thermodynamic properties for the $LiPF_6$ and $NaPF_6$ electrolytes and the comparison with reported data in aqueous electrolytes. For the interested reader, we show exemplary data and intermediate results (the so-called transport factors) in the Supporting Information. At the end of this work, the thus determined ionic transport and thermodynamic properties of the lithium and the sodium electrolytes are used in a simulation of a hypothetical 1D "NMC/graphite" cell (using the characteristic open circuit potential vs capacity and the characteristic kinetics of a lithium-ion battery with NCM and graphite), employing COMSOL Multiphysics® to analyze the effect of the different electrolyte parameters on the discharge behavior of such cells.

Ionic conductivity.—Figure 1a shows the ionic conductivities at 25 °C for 0.1-2 M $LiPF_6$ and $NaPF_6$ in EC:DEC (1:1 v:v). Up to ~1 M concentrations, the electrolyte conductivities for both electrolytes are similar and differ by less than 10%. A maximum conductivity of ~8.0 mS cm^{-1} and ~8.5 mS cm^{-1} is obtained for the $LiPF_6$ and $NaPF_6$ electrolytes, respectively, at ~1 M salt concentrations (the conductivity maximum at ~1 M $LiPF_6$ was also observed for EC:DMC (1:1 w:w) and EC:EMC (3:7 w:w) based electrolytes at 25 °C).[21] Beyond ~1 M concentrations, the electrolyte conductivities start to differ substantially, with higher values for the sodium compared to the lithium ion containing electrolyte (compare blue circles, and purple squares, respectively). At 2 M concentrations, the conductivities of the lithium and the sodium electrolyte have decreased to ~4 mS cm^{-1} and 7 mS cm^{-1}, respectively. The solid lines in Fig. 1a represent the functional approximations of the experimental values to the conductivity equation given in the first column of Table I. Figure 1b shows the conductivities for the aqueous electrolytes with LiCl, NaCl, and KCl (data from Ref. 22 and transformed into molarities with assumed linear densities from Ref. 23). In the aqueous electrolyte, for concentrations below 0.3 M, the conductivities are similar and only start to differ substantially above 0.5 M. At 1 M concentrations, the electrolyte conductivities for the aqueous systems are ~65 mS/cm, ~75 mS/cm, and ~100 mS/cm for LiCl (blue circles), NaCl (purple squares), and KCl (green stars), respectively, and also show an increasing spread for increasing salt concentrations (compare Fig. 1b).

For both aqueous and non-aqueous systems, the same trends are observed at high concentrations, i.e., higher conductivities for electrolytes containing the larger cation. This trend can be explained with different electrolyte viscosities due to weaker interaction between the larger cation and solvent/anion. This is supported, e.g., by the substantially higher viscosities of $LiClO_4$ compared to $NaClO_4$ that are reported above 1 M salt concentrations in PC.[13] In the same publication, analogous behavior is observed as in Fig. 1a, namely similar conductivities at low concentrations and clearly higher conductivities of sodium electrolytes at higher concentrations. In addition, the formation of ion pairs and/or triplets at high salt concentrations may further reduce the number of free charge carriers.[24] The stronger Coulomb forces of the lithium ion would be more likely to bind the PF_6^- anions, forming ion pairs which is in agreement with the observed stronger conductivity decay at high concentrations for the lithium electrolyte. As a corollary, one would expect noticeably smaller ohmic overpotentials at high concentrations for $NaPF_6$ compared to $LiPF_6$ electrolytes when drawing large current densities from a sodium vs a lithium-ion battery.

Binary diffusion coefficient.—The concentration dependent binary diffusion coefficients for $LiPF_6$ and $NaPF_6$ in EC:DEC (1:1 v:v) was obtained using the pulse polarization technique that was initially developed by Harned and French for cells without a porous separator between the electrodes;[25] later on, we had extended this for cells that contain a porous separator and described in detail the various analysis methodologies to extract the concentration dependent binary diffusion coefficient ($D_\pm(c)$).[19] The latter describes the coupled motion of anion and cation along a salt concentration gradient in a binary electrolyte.[26] Applying of a short enough galvanostatic pulse to a symmetric cell (see *Experimental* section) leads to a change of the salt concentration only in the vicinity of the electrodes, accompanied by a change in cell potential; upon the relaxation of the thus produced concentration gradient due to diffusion in a subsequent resting phase, the time dependence of the cell potential allows to calculate the binary diffusion coefficient.

As discussed in Ref. 19, the most reliable determination of $D_\pm(c)$ from pulse polarization methods is an analysis of the time dependence of the long-term potential relaxation (referred to as the $D_\pm|^{\text{pulse}}_{\text{long-term}}$ method in Ref. 19). An outline of the procedure is given in the first part of the supporting information (SI), together with an exemplary data set (Fig. S1) for 1.5 M $LiPF_6$ as well as for 1.5 M $NaPF_6$ in EC:DEC (1:1 v:v). It basically involves plotting the logarithm of the cell voltage after a galvanostatic step (corrected by the long-term offset voltage) vs time, which follows a linear relationship at longer times; the slope in this linear region ($m_{\ln}$) allows to determine the binary diffusion coefficient $D_\pm(c)$ from:

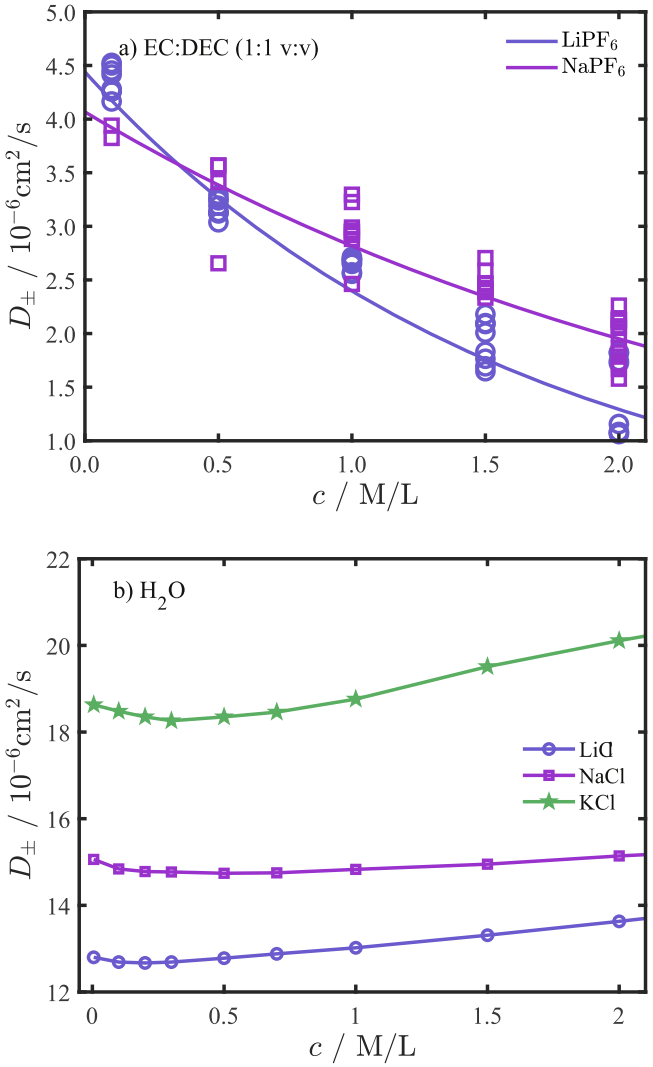

Figure 2. Diffusion coefficients of (a) $LiPF_6$ and $NaPF_6$ in EC:DEC (1:1 v:v, 5 wt% FEC was added to sodium electrolytes in coin cells) determined at 25 °C in symmetric coin cells (as described in the *Experimental* section), using the technique described previously[19] (the data analysis procedure is explained in the Supporting Information); the solid lines represent fits to the equation given in Table I together with the fitting parameters and their confidence intervals; (b) Aqueous LiCl, NaCl, and KCl electrolytes (data are taken from Ref. 27); the solid lines merely serve as a guide to the eye.

$$D_{\pm}(c) = -\frac{\tau_{\text{Sep.}} \cdot l_{\text{Sep.}}^2}{\pi^2} \cdot m_{\ln} \qquad [1]$$

where $l_{\text{Sep.}}$ represents the separator thickness (here, $l_{\text{Sep.}} = 500$ μm) and $\tau_{\text{Sep.}}$ represents the separator tortuosity (here, $\tau_{\text{Sep.}} = 4.8$[21]). For more details about the method, the interested reader is referred to Ref. 19. From the slopes of the long-term potential relaxation curves of repeat pulses (see currents listed in Table S1 in the Supporting Information) and repeat cells at a given concentration (at least 2 cells) we obtained the binary diffusion coefficients depicted in Fig. 2a for $LiPF_6$ (blue circles) and $NaPF_6$ (purple squares) in EC:DEC (1:1 v:v) electrolytes. In the case of the $LiPF_6$ electrolyte, at least four measurements were taken for each cell at a given concentration (resulting from the potential relaxation after four pulses, with alternating current); in the case of the 0.1 M $NaPF_6$ electrolyte, only the potential relaxation after the first pulse could be used for each cell at a given concentration, as the potential relaxations in subsequent pulses showed increasing noise levels and/or random potential jumps, which we ascribe to side reactions and/or the formation of dendritic structures at the sodium metal electrodes.

Figure 2a shows higher binary diffusion coefficients for the $NaPF_6$ compared to the $LiPF_6$ electrolyte at all comparable salt concentrations. At 1 M concentrations, diffusion coefficients of $(2.5 \pm 0.2)\cdot10^{-6}$ cm^2/s and $(2.9 \pm 0.25)\cdot10^{-6}$ cm^2/s are found for $LiPF_6$ and $NaPF_6$, respectively. The found value for 1 M $LiPF_6$ in EC:DEC (1:1 v:v) is slightly lower but still comparable to the values found previously for 1 M $LiPF_6$ in EC:DMC (1:1 w:w) and 1 M $LiPF_6$ in EC:EMC(3:7 w:w) of ~3 to $3.5\cdot10^{-6}$ cm^2/s.[21] Similarly, in the aqueous LiCl, NaCl, and KCl electrolytes, the binary diffusion coefficients follow the same order, viz., K > Na > Li (compare Fig. 2b). In the aqueous electrolytes, the diffusion coefficients are rather constant, while for the non-aqueous EC:DEC (1:1 v:v) based $LiPF_6$ and $NaPF_6$ electrolytes the binary diffusion coefficient decreases monotonically with increasing concentration, consistent with previous reports for binary diffusion coefficients for lithium salts in non-aqueous solvents.[19,28,29] Only at concentrations below 0.5 M the found diffusion coefficient from the lithium/lithium coin cell experiments yielded higher values compared to the sodium case. The observed decrease of the binary diffusion coefficients with concentration in non-aqueous electrolytes may be explained by the generally strongly increasing viscosity of non-aqueous electrolytes for increasing salt concentrations, hindering ion movement. Assuming that the higher viscosities reported by Kuratani et al.[13] for $LiClO_4$ compared to $NaClO_4$ in PC would also hold for $LiPF_6$ and $NaPF_6$ in EC:DEC, the here observed lower diffusion coefficients for $LiPF_6$ compared to $NaPF_6$ in EC:DEC would be expected. In the aqueous system, the viscosity of the electrolyte is not affected strongly by the increasing salt concentration, at least not in the concentration range given in Fig. 2b, explaining the fairly constant binary diffusion coefficient values.

During the operation of a battery, the formation of concentration gradients is unfavorable, as they yield increased overpotentials. The build-up of ionic concentration gradients is counteracted by ion diffusion and, therefore, higher diffusion coefficients reduce overpotentials during operation and are thus beneficial when using thick electrodes and when applying fast charge/discharge rates. The electrolyte property which links concentration gradients to overpotentials is the thermodynamic factor, which is analyzed in the following sections together with the electrolytes' transference numbers.

Thermodynamic factor.—For the determination of thermodynamic factors (TDF) and transference numbers (t_+), we make use of two experimentally obtained transport factors (a and b).[30]

$$a \equiv \text{TDF} \cdot (1 - t_+) \qquad [2]$$

$$b \equiv \text{TDF} \cdot (1 - t_+)^2 \qquad [3]$$

These can be determined from (i) the short-term potential relaxation after galvanostatic pulses in symmetric cells and (ii) the concentration potential measured in concentration cells. A concise summary of this approach is given in Fig. 1 of Ref. 21 (the only difference is that the concentration cell setup used in the present study is that shown in Fig. 1 in Ref. 20 rather than that shown in the middle panel of Fig. 1 in Ref. 21).

Concentration cell potentials (U_{CC}) are measured for pairs of salt concentrations that differ only by a small value (Δc) from a given central value of c_0 (i.e., $c_i = c_0 \pm \Delta c$, further on referred to as "differential concentrations"). Specifically, concentration potentials were measured for the electrolyte concentration pairs 0.065 M–0.1 M, 0.35 M–0.5 M, 0.75 M–1 M, 1.25 M–1.5 M, and 1.75 M–2 M, and the determined U_{CC} values from at least 2 cells are plotted vs the mean concentration c_0 in Fig. S2 (simply referred to as c in the x-axis label). From the U_{CC} values, the transport factor a can be calculated using Eq. 9 in Ref. 21 (reproduced as Eq. S1 in the SI), whereby the thus obtained transport factors a are assigned to the

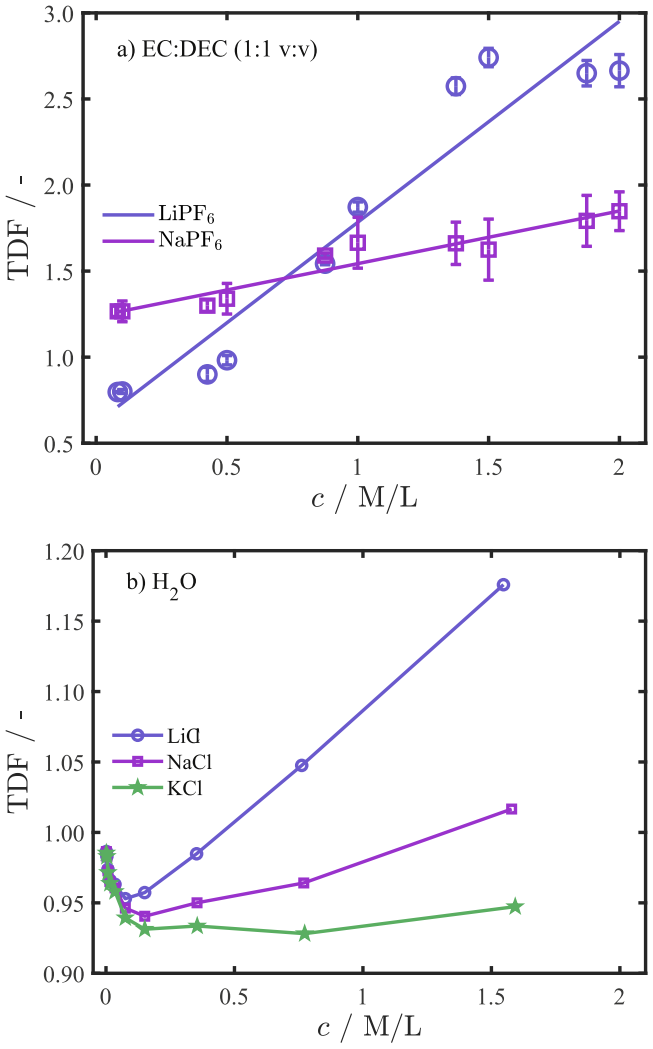

Figure 3. Thermodynamic factors at 25 °C of (a) $LiPF_6$ and $NaPF_6$ in EC:DEC (1:1 v:v, 5 wt% FEC was added to sodium electrolytes in coin cells) determined from the linearly interpolated transport factors a and b shown in Figs. S4 and S5 and defined by Eqs. 2 and 3, using the methodology described in Ref. 21; the solid lines are based on the equation and the parameters given in Table I, while error bars are based on Gaussian error propagation of the standard error of the mean of the transport factors a and b; (b) Aqueous LiCl, NaCl, and KCl electrolytes (data from Ref. 22 and transformed into molarities with assumed linear densities from Ref. 23), solid lines serve as a guide to the eye.

mean concentrations (c_0) of each electrolyte pair (e.g., a for the 0.75 M–1 M concentration pair is plotted at 0.875 M in Fig. S4).

The second transport factor b is determined from the short term potential relaxation of the galvanostatic pulse experiment (for details compare Fig. 1 in Ref. 21), i.e., from the same experiments that were conducted for the above-described determination of the binary diffusion coefficients from at least two cells each. Specifically, calculation of b requires to find the potential established just after the current interrupt from the analysis of the potential transient after the galvanostatic pulses, using the artificial time $1 - \frac{\sqrt{T_I}}{\sqrt{t} + \sqrt{t - T_I}}$, where T_I is the time duration of the current application and t is the time variable starting at the beginning of the current application (see right-hand panel of Fig. 1 in Ref. 21). From extrapolation of the first linear section (x-values below 0.3, see dashed black lines in Fig. S3), the potential established just after the current interrupt ($U(T_1)$) can be obtained. From $U(T_1)$ and the above determined exponential slope of the long term potential relaxation m_{ln}, together with the separator thickness, the electrode area, and the separator porosity, the transport factor b can be determined (see Eq. 11 in Ref. 21, reproduced as Eq. S2 in the SI).

Figures S4 and S5 show the thus determined transport factors a and b for the EC:DEC (1:1 v:v) based electrolytes with $LiPF_6$ (marked by circular symbols) and $NaPF_6$ (marked by square symbols). However, these are obtained at different concentrations (c_0), since the galvanostatic pulse experiments were conducted at 0.1 M, 0.5 M, 1.0 M, 1.5 M, and 2 M salt concentrations, while the concentration cell potentials were obtained at average c_0 values of 0.0825 M, 0.425 M, 0.875 M, 1.375 M, and 1.875 M (based on the above-stated concentration pairs that were chosen to give sufficiently large U_{CC} values). Therefore, since the calculation of the transference number and of the thermodynamic factor from the transport factors requires that the transport factors are known at the same (average) salt concentration c_0 (viz., $t_+(c_0) = 1-b(c_0)/a(c_0)$ and $\mathrm{TDF}(c_0) = a(c_0)^2/b(c_0)^2$, based on Eqs. 2 and 3), the a vs c (Fig. S4) and the b vs c data (Fig. S5) were linearly interpolated to yield a and b pairs at the same c_0 value; the interpolated values of a and b are marked as crosses in Figs. S4 and S5, respectively.

The resulting thermodynamic factors ($\mathrm{TDF}(c_0) = a(c_0)^2/b(c_0)$) for $LiPF_6$ and $NaPF_6$ in EC:DEC (1:1 v:v) shown in Fig. 3a increase with increasing salt concentration. In line with the theoretical definition of the thermodynamic factor, the thermodynamic factor for the most dilute 0.1 M $LiPF_6$ electrolyte is close to unity, and thus in accordance with theory. On the other hand, the analysis of the 0.1 M $NaPF_6$ electrolyte indicates a value for the thermodynamic factor of 1.27. While this value is not in agreement with the theory similar values have been found before[21] and could be explained, for example, with an underestimated diffusion coefficient. The relatively large error bars for the data in Fig. 3a illustrate that the analysis method to determine the TDF is quite sensitive towards small variations in the determined transport factors (compare especially the relatively high scatter for the transport factors b in Fig. S5). The here obtained TDF values for $LiPF_6$ in EC:DEC (1:1 v:v) are quite similar to those obtained for $LiPF_6$ in EC:DMC (1:1 w:w) and EC:EMC (3:7 w:w) determined in our previous work.[21]

We can compare the thermodynamic factors of $LiPF_6$ and $NaPF_6$ the EC:DEC electrolyte with thermodynamic factors calculated from the activity coefficients of LiCl, NaCl, and KCl in H_2O (activity coefficients from Ref. 22 and transformed into molarities with assumed linear densities from Ref. 23) that are shown in Fig. 3b. While for the LiCl and NaCl aqueous electrolytes the thermodynamic factor changes by less than 20% from infinite dilution to 1.6 M, the thermodynamic factor of $LiPF_6$ and $NaPF_6$ in EC:DEC (1:1 v:v) shows a pronounced increase by a factor of ≈2−2.5 in the same concentration range. At higher concentrations (>0.2 M), the increase of the thermodynamic factor with concentration is the more pronounced, as the cation size decreases, both for the aprotic (Fig. 3a) and the aqueous (Fig. 3b) electrolytes. As the thermodynamic factor is a derivative form of the mean ionic activity coefficient ($\mathrm{TDF} \equiv 1+\mathrm{d}\ln(f_\pm)/\mathrm{d}\ln(c)$), which is normalized to its infinite dilution value by definition, the observed higher TDF for the smaller Li^+ cation may be explained with the different relative change of the solvation structure at infinite dilution compared to higher concentrations. Due to its small size, the lithium ion interacts strongly with the solvent molecules, i.e., it has a large solvation shell at infinite dilution, so that a (partial) loss of solvated molecules at increasing salt concentrations due to a decreasing molar salt/solvent ratio may yield a significant increase in reactivity, i.e. an increase of the mean activity coefficient and thus of the TDF when compared to infinite dilution. At the same time, the larger sodium cation shows weaker coordination at infinite dilution due to its larger ion size, and a (partial) loss of solvated molecules can only yield a smaller relative increase in reactivity and thus in TDF. This is supported by theoretical studies showing a 20% smaller desolvation energy of Na^+ in different EC:DMC ratios at low concentration compared to Li^+.[18] Thus, in our understanding the different slopes of the TDFs are mainly caused by the different activities at the reference state (infinite dilution) of the mean molar activity coefficient.

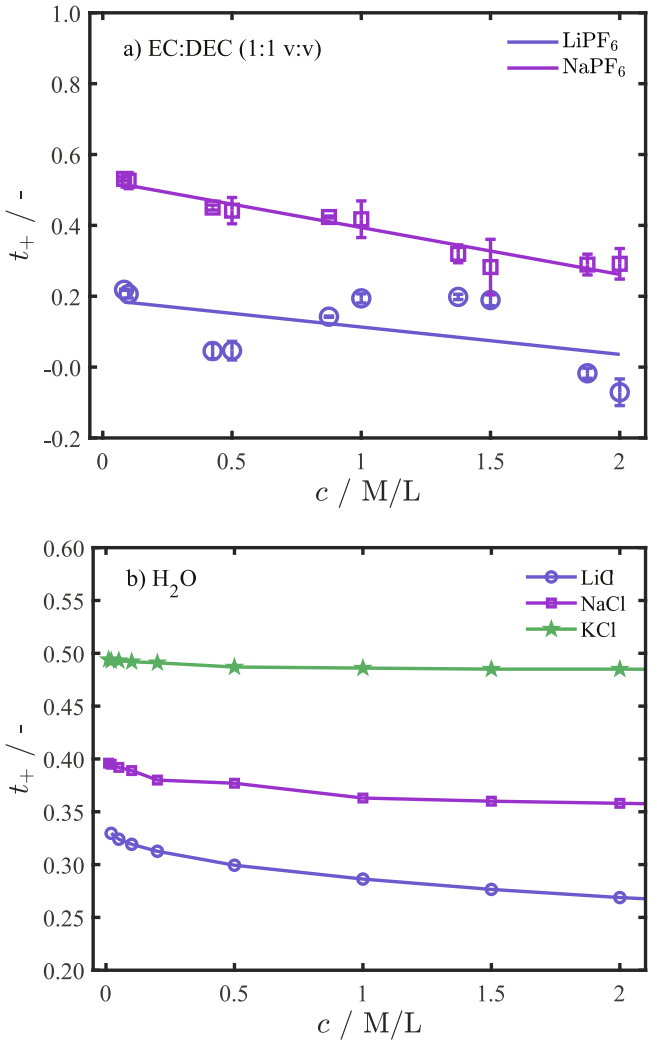

Figure 4. Transference numbers of (a) $LiPF_6$ and $NaPF_6$ solutions in EC:DEC (1:1 v:v, 5 wt% FEC was added to sodium electrolytes in coin cells) determined from the transport factors a and b at 25 °C (based on the data in Figs. S4 and S5), using the methodology described in Ref. 21; the solid lines are based on the equation and the parameters given in Table I, while error bars are based on Gaussian error propagation of the standard error of the mean of the transport factors a and b; (b) Aqueous LiCl, NaCl (18 °C), and KCl electrolytes (data from Ref. 31); the solid lines serve as a guide to the eye.

Transference number.—In analogy to the determination of the thermodynamic factor, the transference numbers in Fig. 4a are obtained from the transport factors a and b ($t_+(c_0) = 1-b(c_0)/a(c_0)$), that are shown in the Supporting Information (Figs. S4 and S5) for the EC:DEC (1:1 v:v) based electrolytes with $LiPF_6$ or $NaPF_6$ (as detailed in Ref. 21). As shown in Fig. 4a, the cation transference numbers for $NaPF_6$ in EC:DEC (1:1 v:v) decrease from ≈0.5 to ≈0.3 and from ≈0.2 to ≈0 for $LiPF_6$ in EC:DEC (1:1 v:v) decreases from concentrations of 0.1 M to 2.0 M. The here obtained t_+ values for $LiPF_6$ in EC:DEC (1:1 v:v) are similar to those obtained for EC:EMC (3:7 w:w), where values of $t_+ \approx 0.3$ at 0.1 M $LiPF_6$ and $t_+ \approx 0.1$ at 2.0 M $LiPF_6$ at 25 °C were obtained.[21] While the trend of decreasing transference number with increasing $LiPF_6$ concentration is the same, the origin of the absolute difference in transference numbers is currently unknown, and it would require a more detailed investigation to clarify the effect of the various solvents (EC, DMC, DEC, and EMC) and their concentrations on the cation transference number in $LiPF_6$ based electrolytes. An inspection of the cation transference numbers of LiCl, NaCl, and KCl in H_2O, shown in Fig. 4b (data from Ref. 31), reveals a similar concentration dependence of the transference number as observed in the aprotic electrolyte (see Fig. 4a), namely a decrease with increasing concentration.

The cation transference number is defined by the ratio of cation mobility to the sum of mobilities of anion and cation.[26] In general, smaller cations have a stronger interaction with aprotic solvent molecules and consequently a larger stokes radius;[12] as this decreases the cation mobility, the transference number of small cations are usually smaller than those of larger cations (assuming identical charges, cations, and solvents). This effect would be expected to be more pronounced at high salt concentrations in aprotic solvents, where strongly solvated ions, such as Li^+ may be strongly interacting with the polar and most strongly solvating EC molecules (in the here used EC:DEC based electrolyte, the molar ratio of EC to $LiPF_6$ at 2 M $LiPF_6$ is ≈3/1). This is consistent with the similar ionic mobilities reported for Li^+ and PF_6^- in DMC, where for increasing EC content the PF_6^- mobility is larger than the mobility of Li^+.[32] As the sodium ion shows a lower interaction with the solvent (smaller charge to radius ratio) and typically has a lower coordination number in aprotic electrolytes compared to the lithium ion,[12] its mobility is less affected at high concentrations.

Similar arguments hold for aqueous electrolytes, except that it must be considered that the molar ratio of solvent/salt is much larger in this case (the molar ratio of H_2O to salt at a 2 M salt concentration is ≈37/1). At infinite dilution, the ionic mobility increases with the ion size (Li < Na < K) and thus supports the order of the transference numbers shown in Fig. 4b.[33] However, due to the still very low molar solvent/salt ratio at 2 M concentrations, the concentration dependence of the lithium ion transference number is much less pronounced in the aqueous LiCl electrolyte (Fig. 4b) compared to the aprotic $LiPF_6$ electrolyte (Fig. 4a). However, for the aqueous alkali chloride electrolytes shown in Fig. 4b, the weak concentration dependence of the cation transference number is clearly higher for Li^+ compared to Na^+ or K^+.

Figure 4a shows higher transference numbers for the sodium system compared to the lithium case. As higher cationic transference numbers mean higher cation mobilities in an electric field, lower concentration gradients and consequentially lower concentration potentials would be expected with the sodium ion based compared to the lithium ion based EC:DEC electrolyte. Before we adopt the found concentration dependent transport properties in a simple 1D Newman model in order to exemplarily show the influence of the electrolyte transport properties, we establish functional approximations for the ionic conductivity, the binary diffusion coefficient, the thermodynamic factor, and the transference number for the EC:DEC (1:1 v:v) electrolyte with $LiPF_6$ or $NaPF_6$.

Functional approximations for the transport and thermodynamic properties.—The concentration dependent ionic conductivity (see Fig. 1a), binary diffusion coefficient (see Fig. 2a), thermodynamic factor (see Fig. 3a), and transference number (see Fig. 4a) for $LiPF_6$ and $NaPF_6$ in EC:DEC (1:1 v:v) were fitted to the empirical functions given in Table I. The empirical function for the ionic conductivity was chosen to fulfill the Kohlrausch square root law[26] at low concentrations and is similar to what we had used in a prior study (compare Eq. 15 in Ref. 21, simply omitting the temperature dependent terms). Similarly, the empirical functions for the other parameters are the same as in Ref. 21, except that the temperature dependent terms were omitted. Although the accuracy of the fitted empirical functions in Table I could be improved by additional measurements, they can be used to estimate the difference in ionic transport for $LiPF_6$ and $NaPF_6$ in EC:DEC (1:1 v:v), using a simple one-dimensional (1D) battery model.

A comparison of the properties of EC:DEC (1:1 v:v) based electrolytes with either $LiPF_6$ or $NaPF_6$ shows somewhat higher conductivities (Fig. 1a), diffusion coefficients (Fig. 2a), and transference numbers (Fig. 4a) for the larger cation (sodium), i.e., the ion with the weaker electrostatic interaction with the solvent molecules. The conductivity and transference number of the $LiPF_6$ based

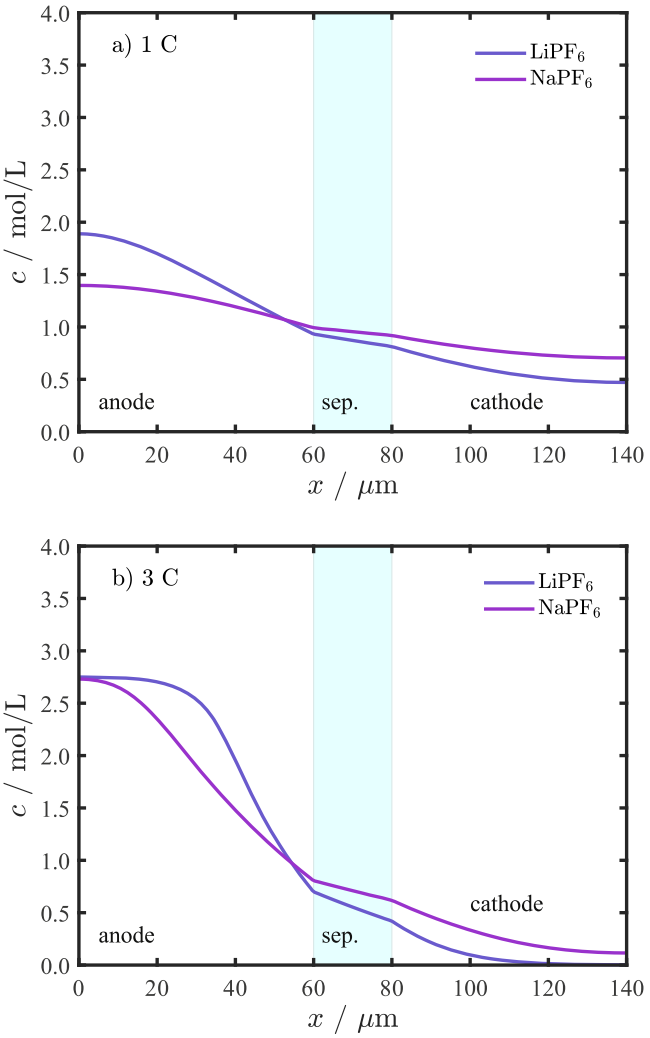

Figure 5. Simulated electrolyte concentration gradients across the cell at the end of discharge (i.e., at a lower cutoff potential of 2.7 V) for a hypothetical lithium/sodium "NMC/graphite" battery (see Table S2): (a) end of 1 C discharge; (b) end of 3 C discharge. The solid lines for $LiPF_6$ (blue) and $NaPF_6$ (purple) in EC:DEC (1:1 v:v) are simulated with the measured ionic transport and thermodynamic parameters given in Table I. Additional simulation parameters are given in Table S2. The separator region is highlighted in cyan to easily discern it from the electrodes (see labels in the figure).

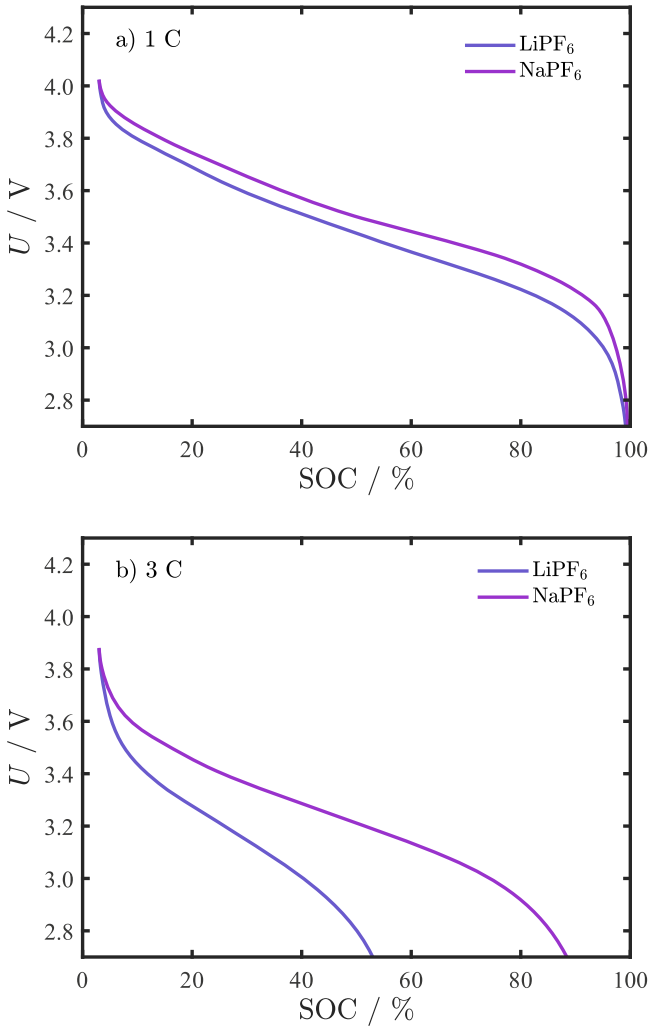

Figure 6. Simulated cell potential vs SOC curves of a hypothetical lithium/sodium "NMC/graphite" cell (using the OCV vs SOC dependence and the kinetic parameters listed in Table S2) during a constant current discharge at different C-rates: (a) at 1 C; (b) at 3 C. Solid lines for $LiPF_6$ (blue) and $NaPF_6$ (purple) in EC:DEC (1:1 v:v) are simulated with the measured transport and thermodynamic parameters given in Table I. Additional simulation parameters are given in Table S2. The initial SOC of 3% was chosen to avoid numerical instabilities at the beginning of the discharge simulations.

electrolyte become increasingly smaller compared to the $NaPF_6$ based electrolyte as the salt concentrations increase to $\geqslant$1 M, which should lead to the development of larger concentration potentials during cell operation for the former. To obtain a more quantitative insight into the effect of the different transport parameters on cell performance, we will next use the concentration dependent transport and thermodynamic parameter relationships given in Table I for 1D simulations of the discharge behavior of a hypothetical lithium or sodium-ion cell.

1D discharge simulations with $LiPF_6$ and $NaPF_6$ electrolyte parameters.—In the following, 0.2 C to 20 C discharge rates of a hypothetical 1D battery cell are simulated using COMSOL Multiphysics® in combination with the empirical functions and fitting parameters listed in Table I to describe the ionic transport and thermodynamic parameters for $LiPF_6$ and $NaPF_6$ in EC:DEC (1:1 v:v). As these parameters have been determined at 25 °C only, the model is isothermal. For the simulation, the kinetic parameters and the open circuit vs state-of-charge relationships for a typical "NMC/graphite" based lithium-ion battery with an areal capacity of 3 mAh cm^{-2} are used and assumed to be identical for the simulated sodium-ion battery (all the parameters and relationships used in the model are summarized in Table S2). While this, of course, is purely hypothetical, it allows to estimate and compare the different ionic transport and thermodynamic parameters of the $LiPF_6$ vs $NaPF_6$ electrolyte on the resulting concentration profiles and the accessible capacity at different rates. To enable this comparison, all the parameters/relationships given in Table S2 are set to identical values for the two cell chemistries. This also means that the same open circuit potentials for the electrodes are used (in this case modeled after graphite and NMC in a lithium-ion battery cell), which is for academic reasons only, as we are of course aware of the fact that the arbitrarily chosen "NMC/graphite" system would not be applicable for the sodium cell chemistry. Additionally, same kinetics are assumed for the simulated sodium and lithium-ion cells although recent research indicates that charge transfer resistances for sodiation may be distinctively larger than for lithiation reactions as observed with hard carbon anodes.[34] Constant current discharge simulations are done at C-rates of 0.2, 0.5, 1, 2, 3, 4, 5, 6, 7, 8, 10, 12, 15, and 20 C until a lower cell cut-off potential of 2.7 V is

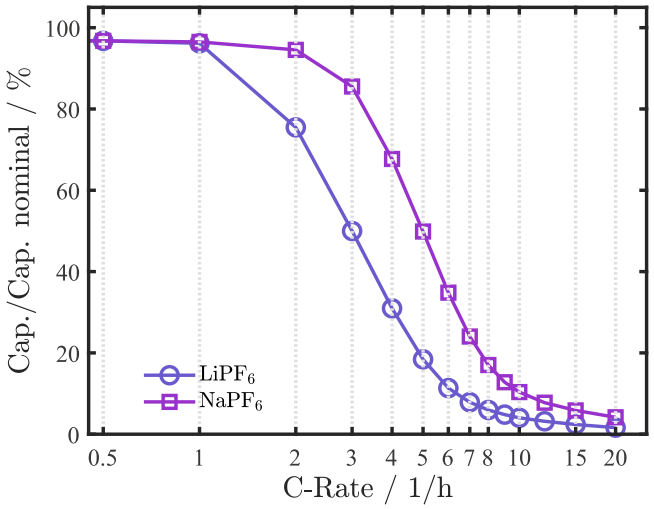

Figure 7. Simulated discharge capacities (referenced to the nominal capacity of the simulated cell setup) at C-rates ranging from 0.5 C to 20 C of a hypothetical "NMC/graphite" cell with $LiPF_6$ and $NaPF_6$ in EC:DEC (1:1 v:v), using the electrolyte parameters given in Table I. Additional simulation parameters are given in Table S2. The initial SOC of 3% was chosen to avoid numerical instabilities at the beginning of the discharge simulations and is the reason for the offset at low C-rates (maximum discharge capacity is 97%).

reached (corresponding to essentially 0% state-of-charge (SOC)). An initial SOC of 3% (see Table S2) was chosen on purpose to avoid numerical instabilities at the beginning of the discharge.

Depending on the current and the electrolyte parameters, larger or smaller concentration gradients may evolve. Exemplary concentration profiles at the end of discharge of the hypothetical cells (i.e., at a cell potential of 2.7 V, the last time step of the simulation) that are based on the electrolyte parameter sets given in Table I and on the other cell parameters given in Table S2 are shown in Fig. 5a for a C-rate of 1 C and in Fig. 5b for a C-rate of 3 C. The corresponding full cell potential curves are shown in Figs. 6a and 6b.

At a C-rate of 1 1/h, as shown in Fig. 5a, the initial 1 M electrolyte concentration increases inside the pores of the anode (as during discharge the alkali ion is deintercalated from the anode) and decreases inside the pores of the cathode (as during discharge the alkali ion is intercalated into the cathode). While the $LiPF_6$ concentrations at the end of a 1 C discharge (blue line in Fig. 5a) at the anode/current collector and at the cathode/current collector interfaces are 1.9 M and 0.5 M, respectively, much smaller concentrations of 1.4 M and 0.7 M are found at the respective interfaces for $NaPF_6$ at the end of discharge (purple line in Fig. 5a). Consistent with the predicted lower concentration gradients in the hypothetical cell with the $NaPF_6$ based electrolyte, the simulated cell voltage vs SOC curve (Fig. 6a) shows a higher cell voltage when using the EC:DEC (1:1 v:v) based electrolyte parameters for $NaPF_6$ (purple line) compared to using those for $LiPF_6$ (blue line), indicating a lower concentration potential for the former. At 50% SOC, the difference in cell voltage (/overpotential) is ≈63 mV (see Fig. 6a). Note that the mere ratio of 1 M electrolyte conductivities would have suggested a reduction of overpotential of the sodium electrolyte compared to the lithium electrolyte of ∼5% (compare electrolyte conductivities of 8.44 mS cm^{-1} and 8.85 mS cm^{-1} for the lithium and the sodium electrolytes at 1 M respectively, see Fig. 1a). Yet even at the moderate discharge rate of 1 C the overpotential is decreased by 30% (OCV at 50% SOC 3.645 V, voltage of simulated cells at 1 C discharge and at 50% SOC: lithium case 3.500 V, sodium cell: 3.437 V) because it does not only contain purely ohmic overpotentials but also included concentration overpotential as well as concentration dependent kinetic overpotentials. This simplistic comparison highlights the necessity to take all electrolyte properties into account when comparing electrolyte transport properties.

As long as the same capacity is obtained for both chemistries, it is straightforward to compare the influence of the transport parameters on the cell behavior. Figure 5a shows a clear trend: smaller concentration gradients for the electrolyte with the larger cation, demonstrating the cumulative benefit of higher conductivity as well as higher transference numbers and binary diffusion coefficients at high concentrations (these dominate over the differences in the thermodynamic factor, as the higher TDF for $LiPF_6$ would otherwise lead to lower overpotentials). The concentration profile at the end of a 3 C discharge as well as the corresponding cell voltage vs SOC curves are shown in Figs. 5b and 6b, respectively. In contrast to the previously shown 1 C discharge with similar discharge capacities for both salts (see Fig. 6a), the discharge capacities at 3 C differ largely between the different cell chemistries (see Fig. 6b), indicating that the difference in electrolyte transport parameters plays an important role and determines the maximum SOC during high C-rate operation. For the 3 C discharge, the SOC after discharge is 50% and 86% for the $LiPF_6$ and $NaPF_6$ electrolyte parameters from Table I, respectively (see Fig. 6b). As a result of the different capacities reached, the concentration gradients at the end of the 3 C discharge shown in Fig. 5b correspond to different amounts of transported charge (and also to different discharge times), and thus cannot be compared directly as done before with the overpotential of the 1 C discharge. Clearly visible is the increased magnitude of the concentration gradients for both cation types at the end of the 3 C discharge (Fig. 5b) compared to the 1 C discharge (Fig. 5a), as well as the pronounced depletion of ions inside the pores of the cathode for the lithium electrolyte at the end of discharge (compare blue $LiPF_6$ concentration gradients in the cathode shown in Fig. 5b at $x >$ 110 μm). Apart from the electrolyte overpotential (concentration overpotential as well as ohmic contributions) for large concentration gradients, this depletion of ions in the pores of either electrode (during discharge in the pores of the cathode, during charge in the pores of the anode) causes a large kinetic overpotential due to the dependence of the exchange current density in the Butler-Volmer equation on the ion concentration.[26] For small ion concentrations, the kinetic resistance becomes very large, i.e., large kinetic overpotentials are necessary to draw/apply the same current. This depletion of ions inside the porous electrodes is the ultimate reason for the drop of usable discharge capacities for higher current rates where the electrolyte is depleted locally.[35]

The simulated discharge capacities (referenced to the full capacity that is accessible at very low C-rates) for the hypothetical "NMC/graphite" cell vs discharge C-rate are shown in Fig. 7. The initial SOC of 3%, which was chosen to avoid numerical instabilities at the beginning of the discharge simulations, is the reason for the finite offset from the y-axis value of 100% at low C-rates. For C-rates up to 1 C, almost identical capacities are reached for both cell chemistries, although at 1 C already rather pronounced differences in the salt concentration gradients can be found (compare Fig. 5a). With the $LiPF_6$ electrolyte parameters, the accessible SOC values steeply drop from >75% to <20% between C-rates of ≈2 C and ≈5 C; the same drop in SOC is observed only for higher C-rates with the $NaPF_6$ electrolyte, i.e., between ≈3.5 C and ≈8 C.

In summary, Fig. 7 illustrates the superiority of the electrolyte transport and thermodynamic parameters of the $NaPF_6$ compared to the $LiPF_6$ electrolyte based on EC:DEC (1:1 v:v) in the modeled hypothetical NCM/graphite cells. As argued before, the difference between the salts is the structure of the solvation shell around the cation, caused by their different interactions with the solvent molecules. Larger cations with equal charge result in weaker interactions with the solvent and lead to higher conductivities at high concentrations, generally higher transference numbers, and higher diffusion coefficients at concentrations above 0.5 M. These trends are the result of the increased mobility of the cation due to the weaker interactions with the solvent molecules. The drop of accessible discharge capacity shown in Fig. 7 correlates with the magnitude of

salt depletion inside the pores of the intercalating electrode (here the cathode); this would, of course, strongly depend on the specific intercalation kinetics, which for this reason were assumed to be identical for both cell chemistries (these hypothetical cell characteristics are listed in Table S2). Our results suggest that based on the electrolyte parameters, higher currents could be drawn from/applied to sodium-ion battery cells compared to lithium-ion batteries without compromising the useable discharge/charge capacity or, alternatively, higher active material loadings could be realized before salt depletion occurs within the electrolyte inside the pores of the porous electrodes.

Conclusions

In this work the ionic conductivity, the thermodynamic factor, the transference number, and the binary diffusion coefficient are determined for $LiPF_6$ and $NaPF_6$ in EC:DEC (1:1 v:v), using previously introduced measurement techniques.[19] The found increase of the ionic conductivity, the cation transference number, and the binary diffusion coefficient, particularly at higher salt concentrations ($\geqslant$1 M) of the $NaPF_6$ electrolyte compared to the $LiPF_6$ electrolyte can be explained with the weaker electrostatic interaction of the larger sodium cation. A qualitative agreement is found for the concentration dependence of these parameters when compared with literature values for aqueous electrolytes containing LiCl, NaCl, and KCl.

In a subsequent 1D cell simulation of a hypothetical "NMC/graphite" cell (i.e., using the characteristic open circuit potential vs capacity and the characteristic kinetics of a lithium-ion battery with NCM and graphite) with an areal capacity of 3 mAh cm^{-2}, we use the two sets of electrolyte parameters to investigate their influence on the cell performance during constant current discharge operation. We show that concentration gradients and associated overpotentials are decreased for the larger cation size. Also, the critical current at which the depletion of the ion concentration within the cathode leads to large kinetic overpotentials is shifted to higher discharge C-rates when the $NaPF_6$ electrolyte parameters are used in the simulation compared to the $LiPF_6$ electrolyte parameters. Although our work neglects different kinetics at the surface of lithium and sodium active materials as well as their different OCV vs SOC relationships, the presented results encourage research in alternative cell chemistries, possibly mitigating some of the rate or areal loading limitations observed for current lithium-ion batteries.

Acknowledgments

J.L., M.G., and H.A.G. gratefully acknowledge the funding by the Bavarian Ministry of Economic Affairs and Media, Energy, and Technology for its financial support under the auspices of the EEBatt project and the BMBF (Federal Ministry of Education and Research, Germany) for its financial support within the ExZellTUM II project (grant number 03XP0081). J. L. thanks Simon Erhard for his initial help with the simulation software COMSOL Multiphysics® and Robert Morasch for rerunningthe simulation with the finally obtained parameter set.

ORCID

Johannes Landesfeind https://orcid.org/0000-0003-0333-2185
Kei Kubota https://orcid.org/0000-0001-8941-3650
Hubert A. Gasteiger https://orcid.org/0000-0001-8199-8703

References

1. N. Yabuuchi, K. Kubota, M. Dahbi, and S. Komaba, *Chem. Rev.*, **114**, 11636 (2014).
2. V. Palomares, P. Serras, I. Villaluenga, K. B. Hueso, J. Carretero-González, and T. Rojo, *Energy Environ. Sci.*, **5**, 5884 (2012).
3. S. Komaba, T. Hasegawa, M. Dahbi, and K. Kubota, *Electrochem. Commun.*, **60**, 172 (2015).
4. R. Dugas, A. Ponrouch, G. Gachot, R. David, M. R. Palacin, and J. M. Tarascon, *J. Electrochem. Soc.*, **163**, A2333 (2016).
5. N. Recham, G. Rousse, M. T. Sougrati, J.-N. Chotard, C. Frayret, S. Mariyappan, B. C. Melot, J.-C. Jumas, and J.-M. Tarascon, *Chem. Mater.*, **24**, 4363 (2012).
6. C. Vaalma, G. A. Giffin, D. Buchholz, and S. Passerini, *J. Electrochem. Soc.*, **163**, A1295 (2016).
7. Y. Marcus, *Pure Appl. Chem.*, **57**, 1129 (1985).
8. L. W. Shacklette, *J. Electrochem. Soc.*, **135**, 2669 (1988).
9. S. Komaba, W. Murata, T. Ishikawa, N. Yabuuchi, T. Ozeki, T. Nakayama, A. Ogata, K. Gotoh, and K. Fujiwara, *Adv. Funct. Mater.*, **21**, 3859 (2011).
10. J. Deng, W.-B. Luo, S.-L. Chou, H.-K. Liu, and S.-X. Dou, *Adv. Energy Mater.*, **8**, 1701428 (2017).
11. P. K. Nayak, L. Yang, W. Brehm, and P. Adelhelm, *Angew. Chemie Int. Ed.*, **57**, 102 (2018).
12. Y. Matsuda, H. Nakashima, M. Morita, and Y. Takasu, *J. Electrochem. Soc.*, **128**, 2552 (1981).
13. K. Kuratani, N. Uemura, H. Senoh, H. T. Takeshita, and T. Kiyobayashi, *J. Power Sources*, **223**, 175 (2013).
14. A. Ponrouch, E. Marchante, M. Courty, J.-M. Tarascon, and M. R. Palacín, *Energy Environ. Sci.*, **5**, 8572 (2012).
15. M. Okoshi, Y. Yamada, S. Komaba, and A. Yamada, *J. Electrochem. Soc.*, **164**, 54 (2017).
16. A. V. Cresce et al., *Phys. Chem. Chem. Phys.*, **19**, 574 (2017).
17. A. Ponrouch, D. Monti, A. Boschin, B. Steen, P. Johansson, and M. R. Palacín, *J. Mater. Chem. A*, **3**, 22 (2015).
18. E. Jónsson and P. Johansson, *Phys. Chem. Chem. Phys.*, **14**, 10774 (2012).
19. A. Ehrl, J. Landesfeind, W. A. Wall, and H. A. Gasteiger, *J. Electrochem. Soc.*, **164**, A826 (2017).
20. A. Ehrl, J. Landesfeind, W. A. Wall, and H. A. Gasteiger, *J. Electrochem. Soc.*, **164**, 2716 (2017).
21. J. Landesfeind and H. A. Gasteiger, *J. Electrochem. Soc.*, **166**, A3079 (2019).
22. W. M. Haynes, *CRC Handbook of Chemistry and Physics* (CRC Press, Boca Raton, FL) 95th ed. (2014).
23. J. A. Gates and R. H. Wood, *J. Chem. Eng. Data*, **30**, 44 (1985).
24. D. M. Seo, S. Reininger, M. Kutcher, K. Redmond, W. B. Euler, and B. L. Lucht, *J. Phys. Chem. C*, **119**, 14038 (2015).
25. H. S. Harned and D. M. French, *Ann. N. Y. Acad. Sci.*, **46**, 267 (1945).
26. A. J. Bard and L. R. Faulkner, *Electrochemical Methods - Fundamentals and Applications* 2nd ed.(John Wiley & Sons, Inc, New York) (2001).
27. R. H. Stokes, *J. Am. Chem. Soc.*, **72**, 2243 (1950).
28. A. Nyman, M. Behm, and G. Lindbergh, *Electrochim. Acta*, **53**, 6356 (2008).
29. L. O. Valøen and J. N. Reimers, *J. Electrochem. Soc.*, **152**, A882 (2005).
30. J. Landesfeind, A. Ehrl, M. Graf, W. A. Wall, and H. A. Gasteiger, *J. Electrochem. Soc.*, **163**, A1254 (2016).
31. E. A. Kaimakov and N. L. Varshavskaya, *Russ. Chem. Rev.*, **35**, 89 (1966).
32. A. von Wald Cresce et al., *J. Phys. Chem. C*, **119**, 27255 (2015).
33. S. Koneshan, J. C. Rasaiah, R. M. Lynden-Bell, and S. H. Lee, *J. Phys. Chem. B*, **102**, 4193 (1998).
34. F. Linsenmann, D. Pritzl, and H. A. Gasteiger, *J. Electrochem. Soc.*, **168**, 010506 (2021).
35. K. G. Gallagher et al., *J. Electrochem. Soc.*, **163**, 138 (2016).